

Inverse Electromagnetic Design of Optical Antennas for Heat-Assisted Magnetic Recording

Samarth Bhargava



Electrical Engineering and Computer Sciences
University of California at Berkeley

Technical Report No. UCB/EECS-2012-248

<http://www.eecs.berkeley.edu/Pubs/TechRpts/2012/EECS-2012-248.html>

December 14, 2012

Copyright © 2012, by the author(s).
All rights reserved.

Permission to make digital or hard copies of all or part of this work for personal or classroom use is granted without fee provided that copies are not made or distributed for profit or commercial advantage and that copies bear this notice and the full citation on the first page. To copy otherwise, to republish, to post on servers or to redistribute to lists, requires prior specific permission.

Inverse Electromagnetic Design of Optical Antennas for Heat-Assisted Magnetic Recording

Samarth Bhargava

Electrical Engineering and Computer Science

University of California at Berkeley

12/14/2012

Abstract

An Inverse Electromagnetic Design algorithm is presented that can efficiently solve for optimal shapes of electromagnetic devices, such as antennas, surface textures and gratings. The algorithm was implemented in software along with techniques to represent non-parametric or freeform shapes, which allow the optimization to explore non-intuitive solutions. This Inverse Design Software was then used to design optical antennas for Heat-Assisted Magnetic Recording to efficiently deliver energy to a sub-wavelength spot. The optical system that is proposed here consists merely of a rectangular waveguide and a planar antenna, a simple and inexpensive solution that outperforms the complicated designs from the key players in the data storage industry.

Inverse Electromagnetic Design of Optical Antennas for Heat-Assisted Magnetic Recording

Samarth Bhargava

Electrical Engineering and Computer Science

University of California at Berkeley

12/14/2012

1. Inverse Electromagnetic Design

For electromagnetics problems, a computational algorithm that is capable of automatically designing optimal geometries of dielectric or metal objects within a given optical system is very desirable. Applications include designing antenna shapes to efficiently deliver optical energy to sub-wavelength spots, designing textures for optimal light-trapping in sub-wavelength thick solar cells, and designing efficient couplers between waveguides and devices in integrated photonics. The Inverse Electromagnetic Design method discussed here originates from work with Owen Miller [1], and some of its development and code implementation is in collaboration with him.

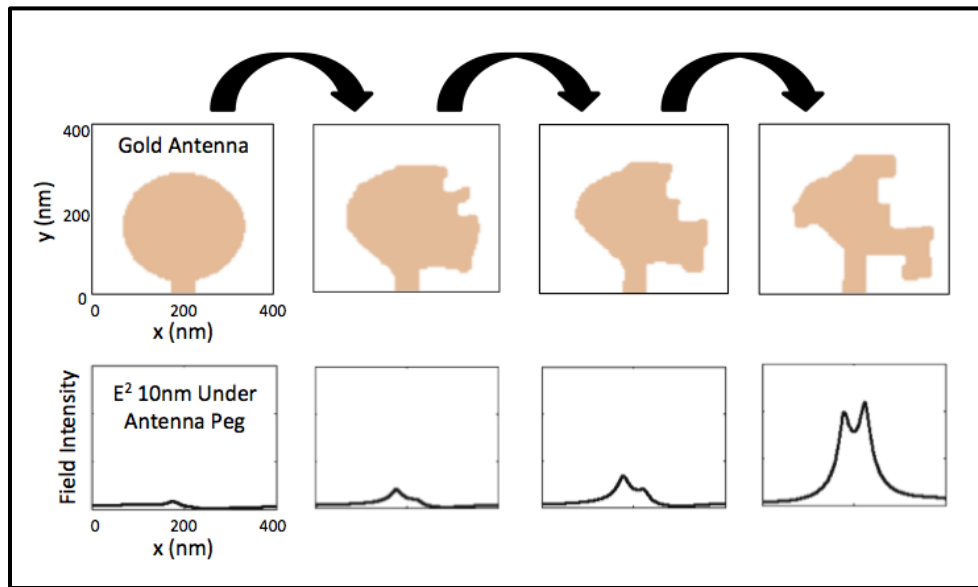


Figure 1: An **Iterative and Creative Inverse Design** of an Optical Antenna's shape. The antenna in the rightmost frame is not likely to be designed without computation and achieves significantly stronger field localization.

Currently, a popular method to optimize very complex structures (i.e. in which there are many geometric parameters) is a genetic algorithm, which by definition is extremely inefficient. This can still be successful for problems where the simulation of the physics is very fast, but this method is not useful for electromagnetic problems since solving Maxwell's Equations in 3-dimensional space is computationally intensive even by today's standards. A more efficient optimization can be achieved with the iterative method of gradient descent, in which one calculates the derivative of the Figure of Merit with respect to each geometric parameter and iteratively changes each parameter to step towards an optimum. This is essentially Newton's Method for a function of many dependent variables. For a complex shape with N geometric parameters, this gradient descent approach requires roughly N simulations per iteration in order to calculate N independent derivatives, one per each geometric parameter. However, optimizing a complex shape with 1000 geometric parameters where each 3D simulation of Maxwell's Equations takes one hour on a High-Performance Computing Cluster is still unfeasible. Thus, current designers in

RF and Optics often limit themselves to simple structures and optimize in a brute force fashion by varying every geometrical parameter in the system (parameter sweeps). With our ability to manufacture devices with subwavelength features and new applications of metal optics today, we no longer should restrict ourselves to simple structures.

The Inverse Electromagnetic Design algorithm proposed here improves on the simple iterative method of gradient descent, which requires N simulations per iteration to calculate a gradient or derivative for each of N geometric parameters. The proposed Inverse Design algorithm exploits symmetries in the solutions of Maxwell's Equations such that the algorithm needs only 2 simulations of Maxwell's Equations per iteration to optimize non-parametric shapes (when N tends to infinity). Because of this efficiency, this algorithm can solve for creative and unintuitive shapes that could not be conceived analytically or qualitatively by an engineer. Figure 2 shows the traditional trade off between number of parameters and computation per iteration of an optimization algorithm. The goal of the proposed Inverse Design method is to break this trade off and greatly reduce the computation required to optimize non-parametric geometries. Figure 1 shows an optimization with the proposed Inverse Electromagnetic Design method that shows that creativity, which I define as exploiting every degree of freedom possible, allows for designs that could not be designed by hand and that offer significantly better performance.

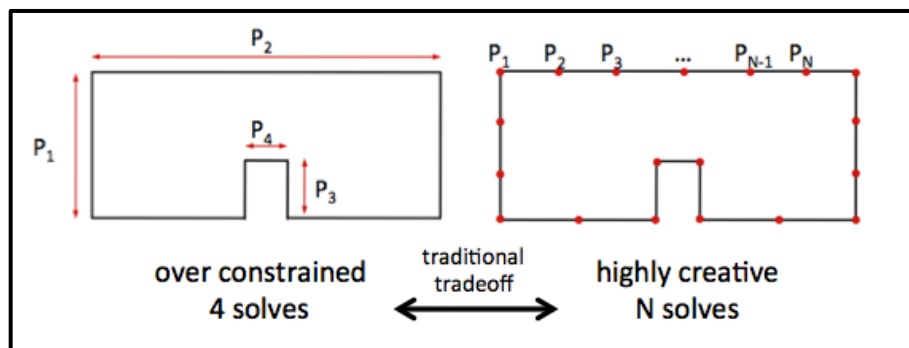


Figure 2: A C-Aperture Antenna can be represented by 4 (left) or N (right) geometric parameters. If confined to a design methodology of parametric sweeps, then more parameters offer more degrees of freedom at the expense of an unreasonable amount of computation (proportional to number of solves).

The proposed Inverse Electromagnetic Design algorithm is described as **Adjoint-Based Gradient Descent**. 'Gradient Descent' is essentially Newton's Method. To find a local maximum or minimum, one simply needs to calculate an instantaneous derivative of a Figure of Merit (FOM) with respect to a Variable and iteratively increment or decrement the Variable until the derivative is zero. A completely freeform shape can be described by having N Variables distributed around the shape's perimeter, where N tends to infinity for an increasingly continuous representation of the shape's boundary, like that in the right frame of Figure 1. 'Adjoint-Based' refers to using symmetries to calculate the derivative of the FOM with respect to all N Variables in an efficient manner. For example, to characterize an antenna, there are two symmetric simulations of Maxwell's Equations. The first involves the antenna being illuminated from the far-field and the localized electric field (the Figure of Merit) is calculated. The second involves the antenna being excited in the near-field and the far-field radiation is calculated. The latter scenario is the Adjoint simulation. How these two simulations can be used to calculate all N derivatives efficiently will be explained the following discussion. Figure 3 shows one iteration of the Adjoint-Based Gradient Descent method. The significant achievement is that only 2 simulations of Maxwell's Equations are required to calculate the Gradient, a collection of derivatives with respect to changes in the shape's boundary. Positive (red) and negative (blue) gradients indicate where the boundary should be pushed outward or inward in order to navigate toward a local optimum in the shape parameter space.

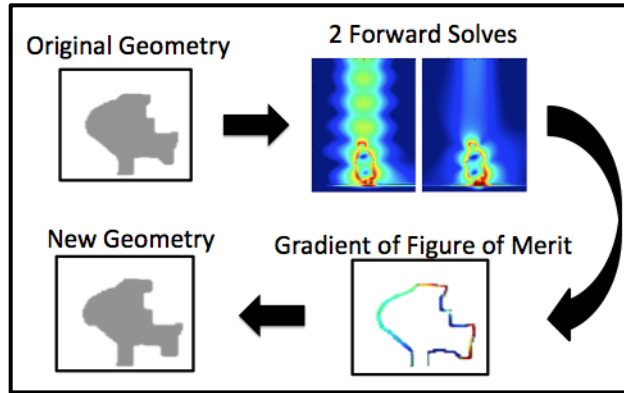


Figure 3: One iteration of **Adjoint-Based Gradient Descent**.

The inefficient way to implement a Gradient Descent optimization of a non-parametric or freeform shape in Electromagnetics is to simply simulate every possible boundary perturbation to a shape and evaluate a Figure of Merit (FOM), which could be any function of Electric and Magnetic fields, for each perturbation. After calculating the change in Figure of Merit (ΔFOM) for every boundary change, one can iteratively change the shape's geometry in a smart way to seek a local optimum. Figure 4 depicts a brute-force optimization of an antenna, where the FOM is function of electric field at location x_0 . To complete one iteration of Gradient Descent, one must calculate ΔFOM for every possible perturbation, which are represented here as boundary deformations at every point x' around the antenna's boundary. This requires N simulations to evaluate a perturbation at each of the N locations of x' .

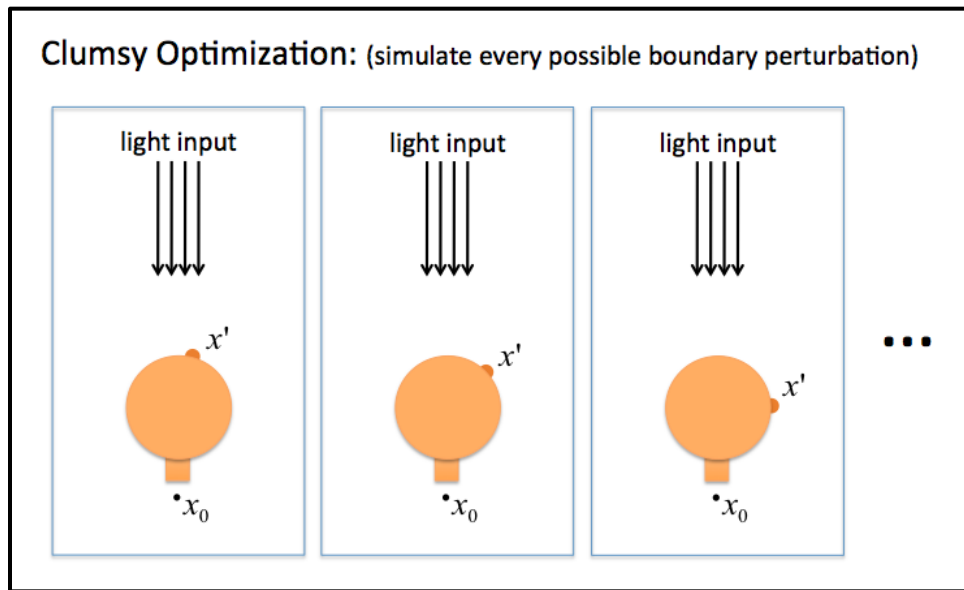


Figure 4: An inefficient way to calculate the change in Figure of Merit due to every possible boundary change is the brute-force method, ie. calculate and simulate every possible boundary perturbation.

Shown in Figure 5, the first key trick to simplify the size of this optimization problem is to approximate the effects of a perturbation to the shape's geometry. The external source induces an electric field in the perturbation (a localized change in epsilon) that oscillates at the electromagnetic frequency. If the perturbation is small enough, then it will only support the dipole resonance mode and will thus act as a **dipole scatterer**. Hence, we can approximate the effect of a perturbation at any location x' with a point current source J_1 at x' and solve Maxwell's Equations to determine the electric field distribution E_1 everywhere in the volume. To evaluate ΔFOM for a perturbation at x' , one must simply observe $E_1(x_0)$, the electric field produced by the respective current source at x_0 . This simulation no longer requires simulating the light source and each physical geometric change as shown in Figure 4.

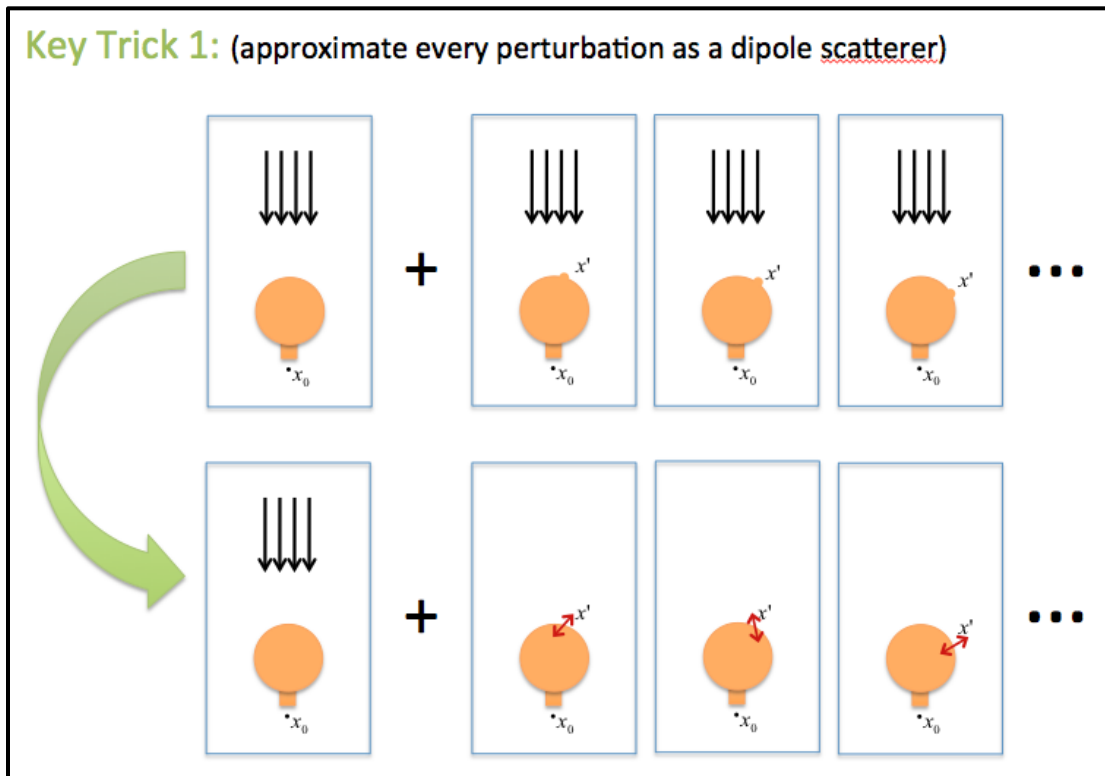


Figure 5: Model every possible perturbation (addition or removal of material) as a **Dipole Scatterer**, whose dipole moment is proportional to the electric field induced in the perturbation.

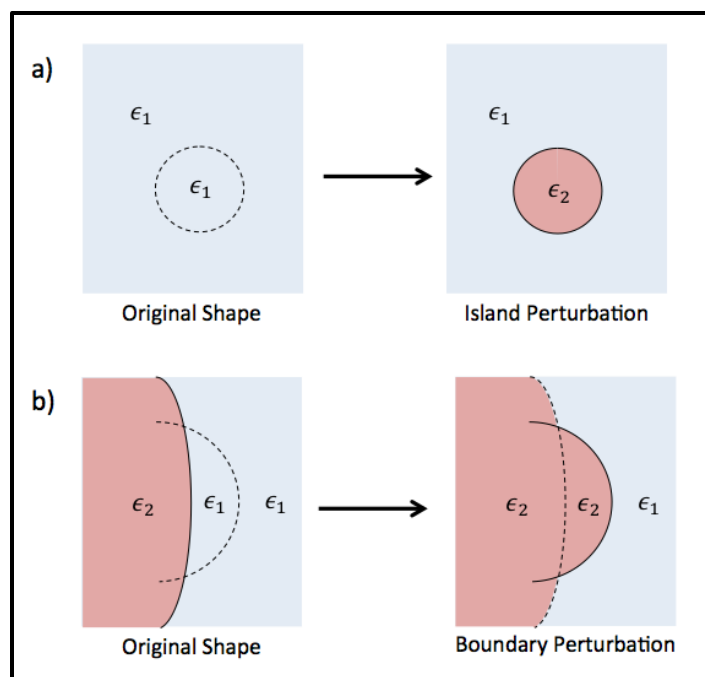


Figure 6: Two types of geometrical perturbations: a) change in epsilon from the inclusion of an isolated island of material; b) change in epsilon from the small deformation of the boundary of a large object of material.

As shown in Figure 6, there are two types of geometric perturbations in a two material system, consisting of permittivities ϵ_1 and ϵ_2 . For the perturbation shown in Figure 6a, if \vec{E}_{orig} is the electric field induced by a light source at location x' , then the dipole moment from the inclusion of a sphere of ϵ_2 at x' is proportional to the \vec{E}_{orig} by the Clausius–Mossotti factor, as shown by the popular Jackson's Classical Electrodynamics [2],

$$\vec{P} = 3 \frac{\epsilon_2 - \epsilon_1}{\epsilon_2 + 2\epsilon_1} \vec{E}_{orig} V_{sphere}$$

For the boundary perturbation shown in Figure 6b, the simplest approximation for the dipole moment induced by a boundary deformation at location x' is calculated as followed. The electric field \vec{E}_{new} in the boundary deformation of ϵ_2 is the original electric field plus some change in field, while taking into account boundary conditions of the parallel and perpendicular components of electric field.

$$\vec{E}_{new} = (\vec{E}_{orig\parallel} + \delta\vec{E}_{\parallel}) + \frac{1}{\epsilon_2} (\vec{D}_{orig\perp} + \delta\vec{D}_{\perp})$$

The dipole moment induced in the boundary deformation follows as the change in dielectric constant in the volume of the perturbation multiplied by this \vec{E}_{new} . The changes in field, $\delta\vec{E}_{\parallel}$ and $\delta\vec{D}_{\perp}$, tend to zero in the limit of the deformation being small, and hence the dipole moment of a boundary perturbation at x' is given by

$$\vec{P} \cong \left\{ (\epsilon_2 - \epsilon_1) (\vec{E}_{orig\parallel}) + \frac{1}{\epsilon_2} (\epsilon_2 - \epsilon_1) (\vec{D}_{orig\perp}) \right\} V_{perturbation}$$

A similar expression is also found, albeit in a more complicated form, by Johnson et. al. in studying perturbation theory of Maxwell's Equations [9] and roughness losses in waveguides [10]. In order to calculate the dipole moment induced in every possible perturbation, one only requires to know \vec{E}_{orig} at every x' , which can be calculated in one simulation of the geometry illuminated by the light source (the left most frame in Figure 5). After performing this first key trick, one still needs to perform many simulations to calculate the electric and magnetic field at the observation point x_0 due to the approximate dipole moment at every x' , to calculate the ΔFOM due to the perturbation.

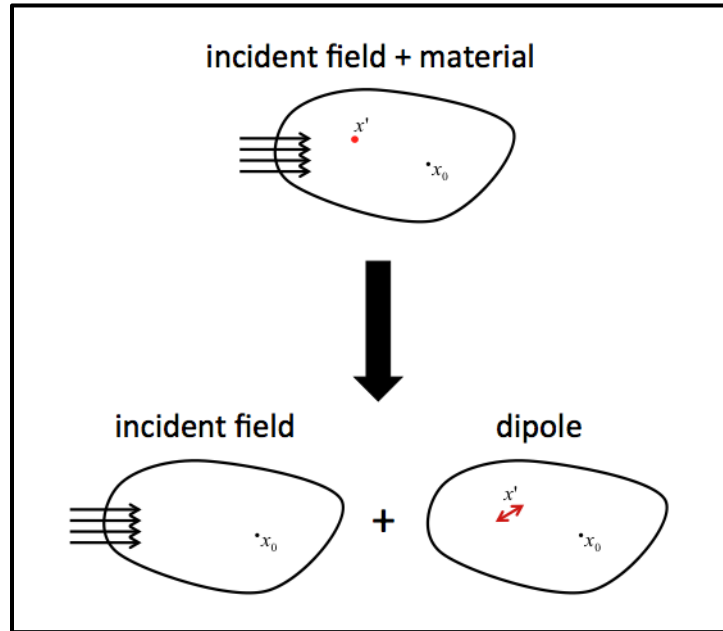


Figure 7: A simulation of Maxwell's Equations to model an insertion of material under an incident light source can be modeled by two separate simulations: one excited with the incident light source and the other excited by a dipole to mimic the material change.

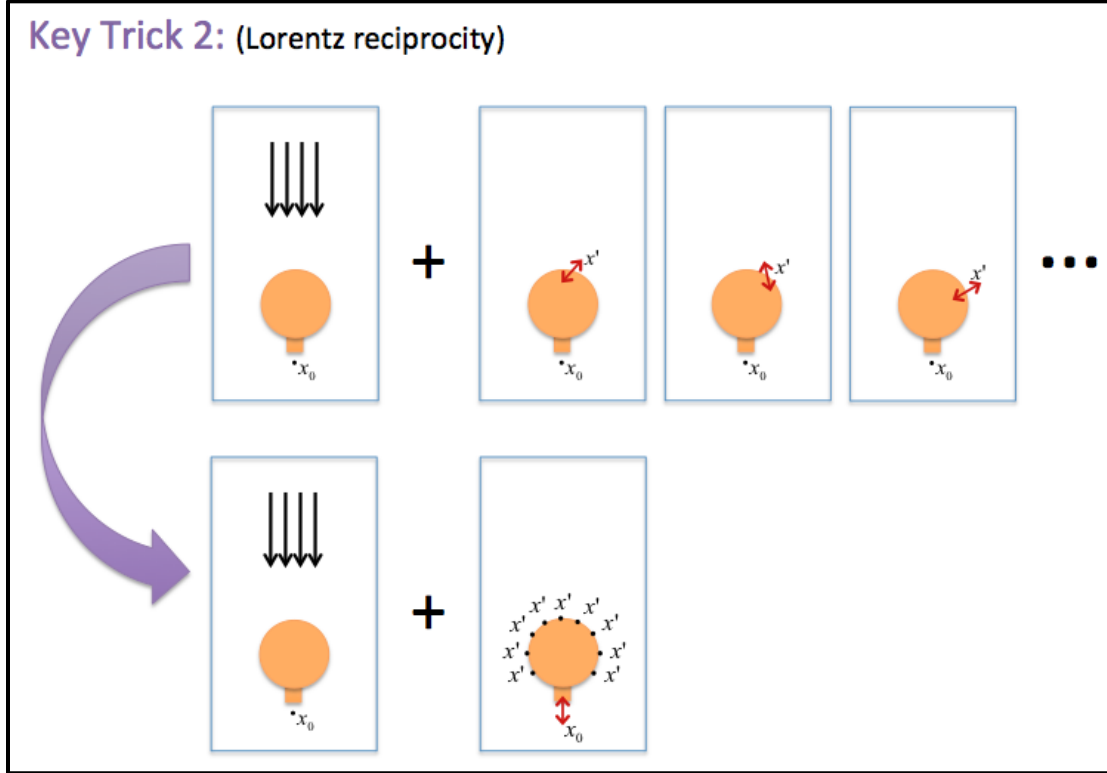


Figure 8: **Reciprocity** parallelizes the calculation of the Green's Function between x' and x_0 .

Shown in Figure 8, the second key trick uses **Lorentz Reciprocity** to greatly simplify the calculation of the electric and magnetic field contributions to location x_0 from every possible perturbation or dipole scatterer. Consider the scenario of two possible current sources J_1 and J_2 that independently produce electric field distributions E_1 and E_2 , respectively, in a volume of arbitrary materials. The simplest form of Lorentz Reciprocity dictates

$$\int J_1 \cdot E_2 \, dV = \int J_2 \cdot E_1 \, dV$$

The induced dipole moment in a geometrical perturbation at x' is equivalent to a point current source J_1 at x' , which produces the electric field distribution E_1 in the entire simulation volume. Also, consider the same volume instead excited with a point current source J_2 at the observation point x_0 which produces the electric field distribution E_2 . The previous Reciprocity relationship becomes

$$J_1 \cdot E_2(x') = J_2 \cdot E_1(x_0)$$

Rather than solving for the electric fields E_1 everywhere in the volume V produced by a current source at x' to evaluate $E_1(x_0)$, one could alternatively solve for the fields E_2 from a current source at x_0 . Using the relationship above, one can calculate $E_1(x_0)$ by instead observing $E_2(x')$ and knowing the currents J_1 and J_2 . The advantage is that from one simulation with a current source J_2 at x_0 , one knows $E_2(x')$ for every x' in the simulation volume. Hence, from this one simulation one can calculate $E_1(x_0)$ and therefore evaluate $\Delta FOM(E_1(x_0))$ for all perturbations at any x' in the volume. Now, the problem has been greatly simplified as we can calculate the gradient everywhere in space from one simulation where we excite the geometry with current sources at the same locations as where the Figure of Merit is evaluated.

This relationship is also well understood from the study of Green's Functions. Essentially, every time one models a perturbation at x' as a dipole scatterer or current source, one solves Maxwell's Equations to determine the function $G_{x' \rightarrow x_0}(J)$, that relates a current J at x' to an electric field at x_0 . The reciprocity of Green's Functions is essentially a simplified case of Lorentz Reciprocity as well. $G_{x' \rightarrow x_0}(J)$ and $G_{x_0 \rightarrow x'}(J)$ are equivalent for an arbitrary volume of

geometries and materials, and one can perform either simulation to determine the other. As depicted in Figure 9, this simply means that the field observed at x_0 from a current J at x' is the same as the field observed at x' from a current J at x_0 .

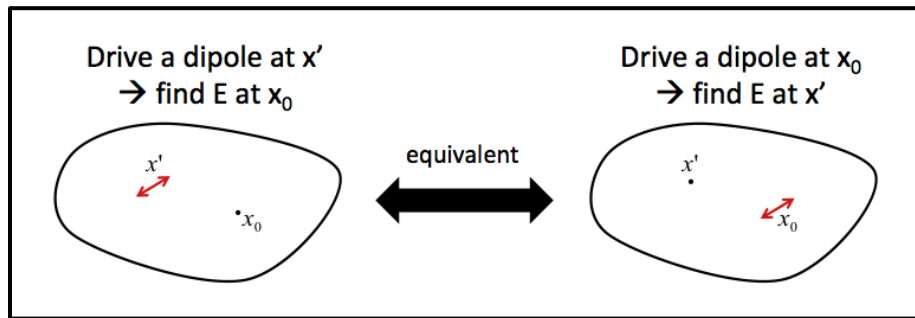


Figure 9: Rayleigh-Carson Reciprocity (a simple case of Lorentz Reciprocity) dictates that the locations of a current source and observation point are interchangeable in an arbitrary system of objects and materials.

Figure 10 shows why there is an efficiency to be gained in solving for the gradient of many geometric parameters in Electromagnetics. The inefficient method from Figure 4 requires solving Maxwell's Equations everywhere in the volume for every possible perturbation at all x' , even though the Figure of Merit is only a function of the fields at x_0 . Essentially, in each of these simulations we are calculating and throwing away field data that is not of interest. However, in this reciprocal or adjoint simulation, every field data point that is calculated is used to evaluate the gradient at those respective x' locations.

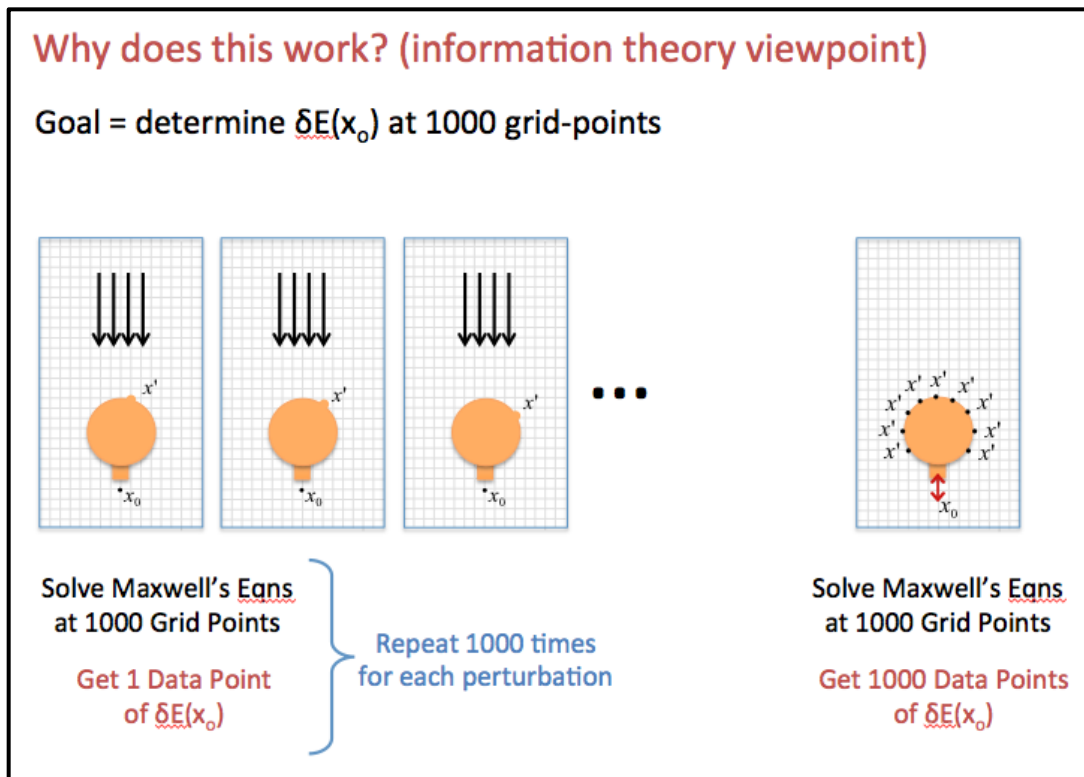


Figure 10: An information theory viewpoint of the Inverse Electromagnetic Design method, which cleverly avoids intensive computation for unneeded data and parallelizes the calculations for all necessary quantities.

In a joint software project with Owen Miller, I developed code to exploit these two key tricks to implement an efficient Inverse Electromagnetic Design algorithm. I do not discuss here, but to take advantage of the gradients calculated by this Inverse Design algorithm, much of my work was to develop software techniques to represent geometries in a completely non-parametric way without using the signed-distance function and the popular Level Set Method. This way of representing ‘freeform’ geometries allows for the Inverse Design software to design nearly all types of electromagnetic devices. Results from applying this software specifically to Optical Antenna designs toward Heat-Assisted Magnetic Recording are discussed in the third section.

2. Heat-Assisted Magnetic Recording (HAMR)

Less well known than Moore’s Law is Kryder’s Law that states that areal storage density increases exponentially, historically, at an even faster rate than that of transistor counts. In magnetic storage, the core of this growth comes from shrinking the size of magnetic domains. The simple Scientific American [11] cartoon in Figure 11a shows an electromagnet, a magnetic yolk excited by a current loop, floating above concentric rings (tracks) of bits. In reality, the surface of a magnetic hard disk consists of sea of randomly sputtered islands of magnetic material (ex: FePt). Due to the variation of the sizes and shapes of these magnetic islands, a group of neighboring islands are used collectively represent a single bit. In the case of perpendicular recording as shown, each collective domain has a static magnetization directed up or down. In order to rewrite data, the electromagnet that flies above the rotating disk must produce a magnetic field greater than the magneto-crystalline anisotropy field contained in the domain, the strength of which is quantitatively described by the coercivity of the material. The difficulty in scaling areal density is that the integral of the anisotropy field per domain correspondingly decreases with smaller sizes of magnetic domains. This causes the domains to be thermally unstable, meaning stored data would not be retained. Hence, to continue scaling, one must increase the coercivity of the magnetic material and, respectively, increase the magnetic field applied by the electromagnet to preserve the functionality of writing data. Recently, current technology has reached magnetic field saturation in the metal comprising of the tip of the electromagnetic write-pole, and hence a stronger electromagnet cannot be created for an ever-shrinking bit size. Figure 11b shows a cartoon of Heat-Assisted Magnetic Recording (HAMR), a technique to use light to heat a single bit to temporarily allow the relatively weak electromagnet to successfully change the magnetization direction of the magnetic domains. Considering that the size of each bit is on the order of $30 \times 30 \text{ nm}^2$, delivering intense light to a deep sub-wavelength spot is not a trivial endeavor as suggested in this popular-press depiction [11]. Although this level of confinement cannot be achieved through conventional optics, it is well within the reach of plasmonics. The dispersion relation for a surface wave on a metal-dielectric interface allows for wavelengths less than 10 nm.

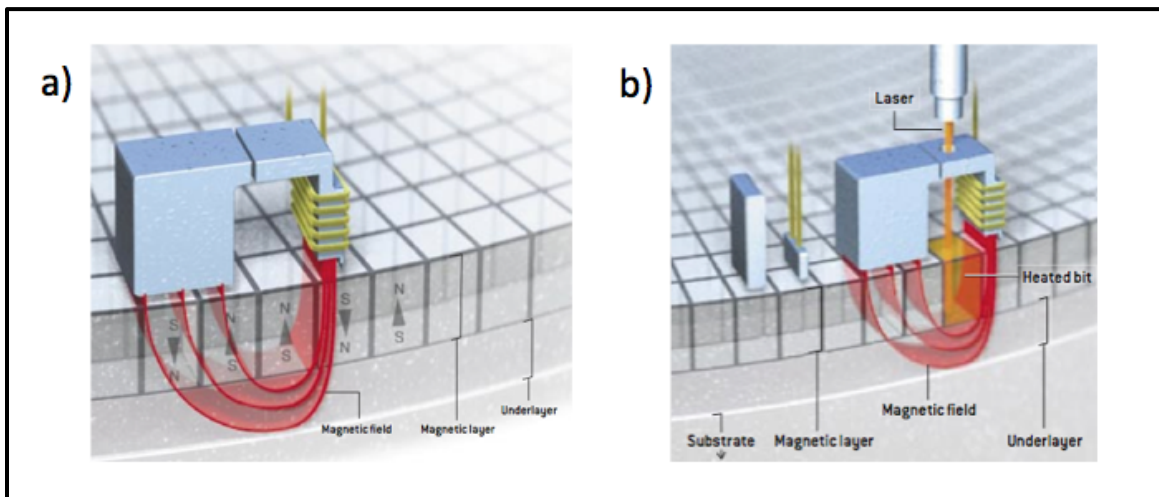


Figure 11: Cartoons by Scientific American [11] of (a) perpendicular recording (b) heat-assisted magnetic recording.

Previous work achieved the focus of optical energy to a 10 nm spot size with gold-coated tapered optical fibers, now used in Near-Field Scanning Optical Microscopes (NSOMs). However, tapered fibers are remarkably inefficient, and typical optical transmission to a sub-100 nm spot is on the order of 10^{-5} to 10^{-7} which severely limits the scan

rate to 10 $\mu\text{m/s}$ or less [3]. The HAMR data-recording scheme relies on focusing optical energy to locally heat the area of a single datum, approximately a hundred square nanometers on the hard disk. In order to write data with a scan rate of up to 10 m/s, the optical system must heat the media by 200 K within 1 ns which amounts to ~ 1 mW delivered to a 30 nm spot [4,5]. Hence, for practical diode laser powers, the system must achieve an energy coupling efficiency of at least 5% or 10^5 times the transmission of tapered fiber. This also represents 10^2 to 10^4 times more power than typical electron-beams, which provide 0.1 to 10 μW [6]. Figure 12 shows a rough comparison of the power requirements of various systems that provide highly confined energy delivery. Moreover, the optical system for HAMR must be fabricated on the same integrated chip containing the electrical and magnetic elements of the hard drive's read/write head. After all, the optical hot spot and the magnetic hot spot must be perfectly aligned.

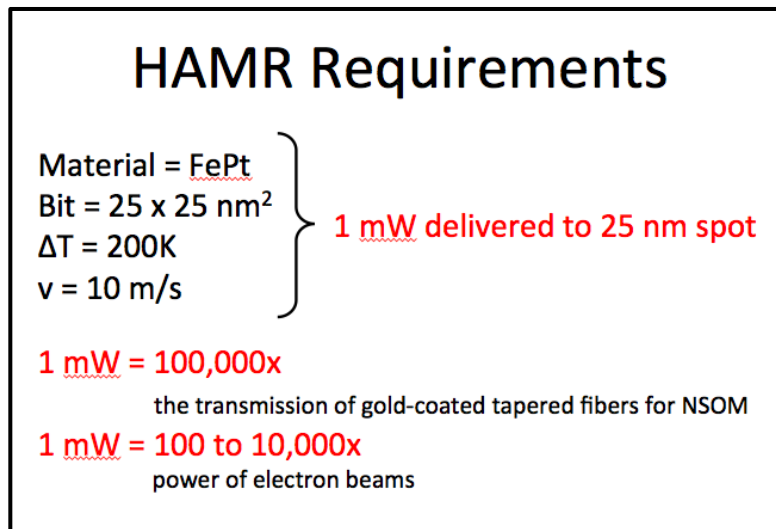


Figure 12: HAMR requirements for **sub-wavelength energy delivery**

In Figure 13, we show several optical antenna geometries investigated for application to HAMR [4,5,7,8]. The peg or ridge of these antennas would be exposed to the air-bearing surface several nanometers away from the hard disk media, such as that shown in Figure 20, with the goal of heating a small volume of the storage layer. Among the presented antennas, the planar lollipop or disk antenna is the simplest to fabricate. Seagate's experimentally demonstrated disk antenna is sized to support the quadrupole mode, which requires illumination from two directions with a 180° relative phase shift between the two beams. Shown in Figure 14, Seagate demonstrated a planar solid immersion mirror [4,5], which is a parabolic dielectric slab with reflective gold-coated edges. Light is coupled into this parabolic condenser by two phase-shifted grating couplers. However, this scheme is challenging to realize because of the difficulty in controlling the phase of two beams of 800 nm light through a $100 \mu\text{m}$ slab waveguide. Although the C-Aperture [7] and 3-Dimensional Taper [8] can be excited simply via butt coupling a rectangular waveguide, fabricating the non-planar antenna itself is very challenging.

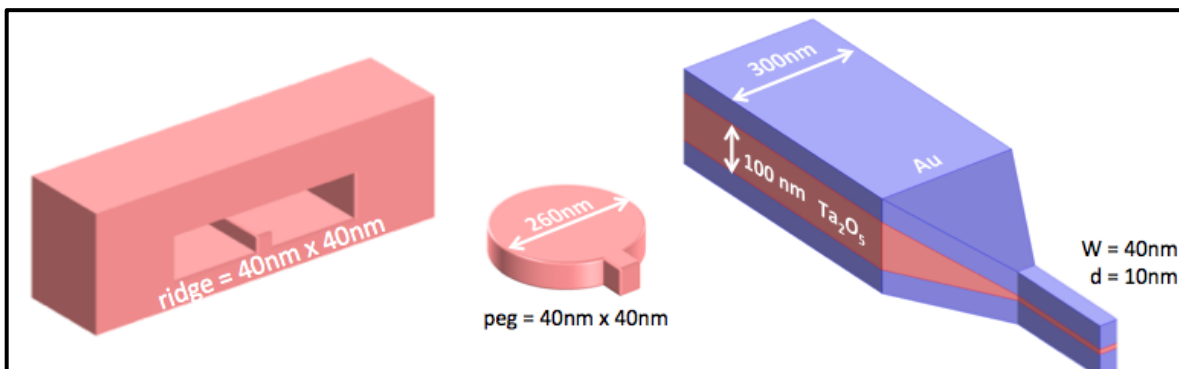


Figure 13: Various optical antenna geometries investigated for HAMR [4,5,7,8].

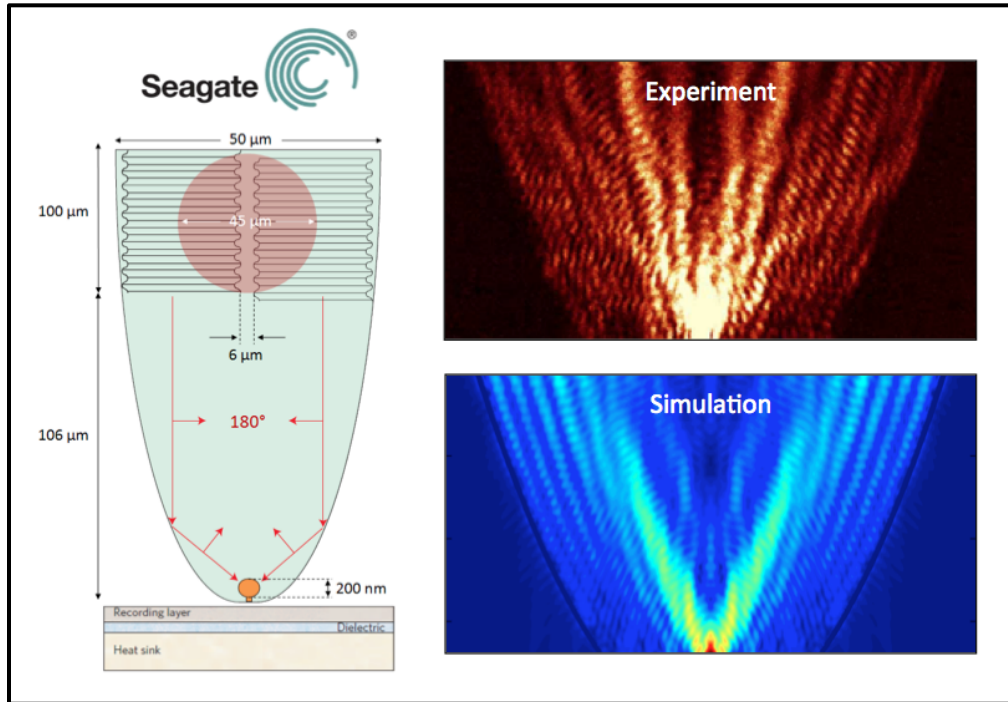


Figure 14: Seagate's HAMR optical system: a parabolic slab waveguide that focuses with two beams with a 180° relative phase offset and excites a quadrupole disk antenna coupled to the hard disk media [4,5].

3. A Simple Solution for Sub-Wavelength Energy Delivery

This final section discusses results from FDTD electromagnetic simulations and the application of the proposed Inverse Electromagnetic Design algorithm to finding a better solution for HAMR. A simpler optical system for HAMR may be a planar antenna excited by a rectangular waveguide, as shown in Figures 15 and 16. There are many advantages to using a rectangular waveguide versus Seagate's parabolic condenser: easier coupling from a Laser, simpler fabrication and no requirement of phase matching. Another advantage, not shown in this paper's graphics, is that a single waveguide can easily circumnavigate the magnetic write-pole, which is integrated on the same chip as the optical system. The magnetic write-pole in Seagate's HAMR system in Figure 14 actually pokes through the middle of the parabolic slab waveguide between the grating couplers and the antenna, partially blocking the intended light path.

The difficulty in designing an optical system that uses a rectangular waveguide is to determine what antenna will radiate with a mode profile similar to a waveguide mode. This seemingly simple question has prevented previous works from implementing a simple planar antenna but rather studying more complicated shapes like the 3D taper or C-Aperture antenna [7,8], neither of which can be made in a simple top-down process. The key design decision for a useful planar antenna to couple with the waveguide is to use a large antenna, one that supports a higher-order resonance mode like the hexapole or octopole modes. Antennas used by Seagate are commonly a quadrupole. These higher-order resonance modes offer opportunity for a very directive antenna and offer a better impedance match between the waveguide and the antenna's high-impedance load, a tiny volume of the hard disk media. The initial antenna shapes that were supplied to the Inverse Electromagnetic Design software was a flat 40 nm gold layer with the simple pattern of a $650 \times 150 \text{ nm}^2$ rectangle (antenna arm) and a $50 \times 50 \text{ nm}^2$ square (antenna peg or tip), shown floating above the waveguides in Figures 15 and 16.

The shapes of the optical antennas were optimized for both cases of illumination, TE and TM rectangular waveguide modes. The Figure of Merit to characterize antenna performance for HAMR was taken as electromagnetic absorption in $100 \times 100 \times 10 \text{ nm}^3$ of the storage layer of the hard disk media, whose layers are shown in Figure 20,

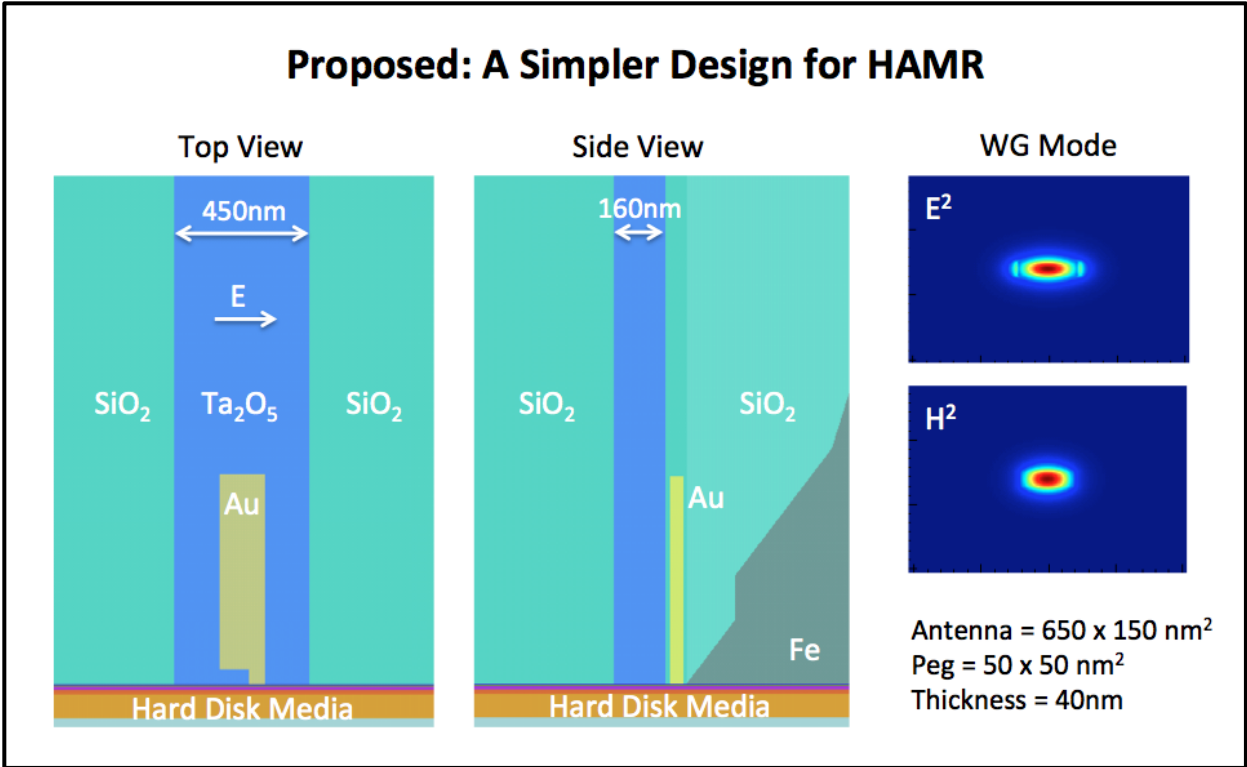


Figure 15: **A simple solution for Heat-Assisted Magnetic Recording.** The proposed system consists of a planar gold antenna floating 20 nm above a TE rectangular waveguide. The magnetic write-pole tip is modeled as a tapered chunk of Iron approaching the hard disk 10 nm above the antenna.

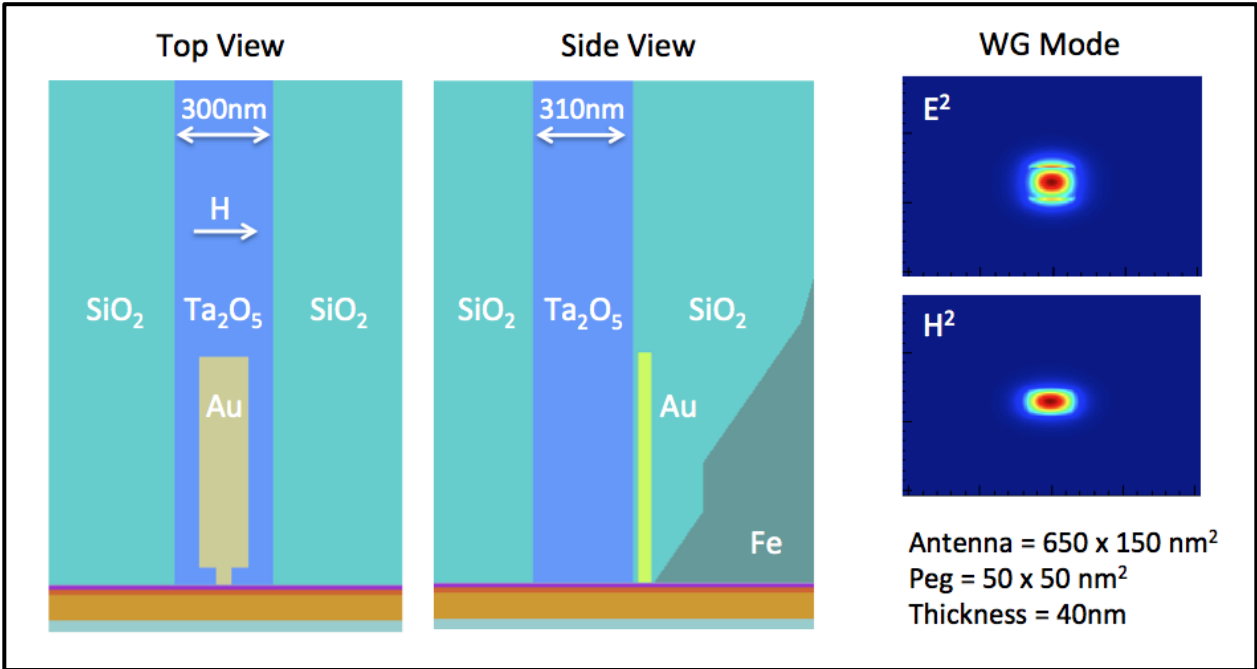


Figure 16: The sister design to that in Figure 15, an optical system consisting of a planar gold antenna floating above a TM rectangular waveguide.

divided by the incident power injected into the waveguide mode. The only part of the geometry that was changed was the 2D cross-sectional shape of the antenna. In all of the optimizations shown here, the width of the peg, the dimension that ultimately determines the optical hotspot dimension, was fixed to 50 nm to allow for better comparison with other work.

Figure 17 shows the iterative evolution of optical antenna shapes for both the TE (above) and TM (below) excitation modes. Note that coupling to the TE mode requires an asymmetric antenna. In both cases, an improvement in absorption within the optical hotspot of the hard disk's storage layer increased from approximately 3% to 8%. These calculations take into account the effects of a large Iron write-pole whose tip is 10 nm above the top surface of the antenna. In Figure 18, cross-sections of the simulated electric field intensity inside the storage layer show the optical hotspot of the initial and optimal antennas, excited by the TM waveguide.

A challenge for all plasmonic devices is that metals are extremely lossy at optical frequencies. The TM-coupled antenna absorbs ~30% of the light injected into the waveguide (comparable to the Seagate's lollipop antenna). Interestingly, after the Inverse Design of the antenna, the absorption in the antenna did not increase. Hence, the ratio of antenna absorption by hard disk media absorption decreased from approximately 10 to 4, which suggests that a less aggressive heatsink may be used to prevent the antenna from melting under operation.

Figure 19 shows a comparison of the optical antennas studied and designed in this work with other published designs. In this comparison, the media absorption efficiency is shown for a range of lengths of the antenna's tip. In all HAMR integrated optical and magnetic chips, the antenna abuts the air-bearing surface, which is exposed by a lapping process. Hence, the antenna's performance for a +/- 10 nm tolerance of this lapping depth is an important metric for practical use by the data storage industry.

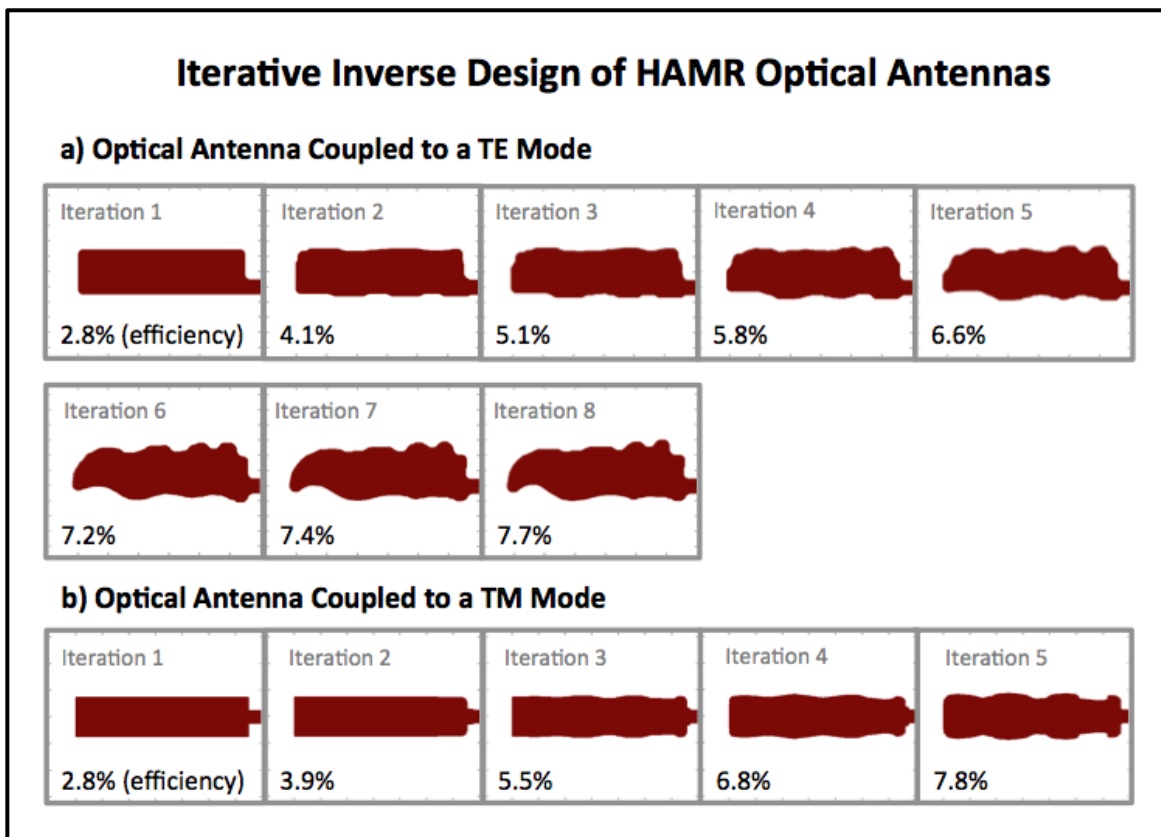


Figure 17: The iterative Inverse Design of the cross-sectional shape of Optical Antennas for HAMR. The Figure of Merit that is optimized is the efficiency of absorption within the optical hotspot in the storage layer given a fixed power injected into the waveguide. The optical system was modeled in Lumerical FDTD as shown in Figure # for both the TE and TM rectangular waveguide systems.

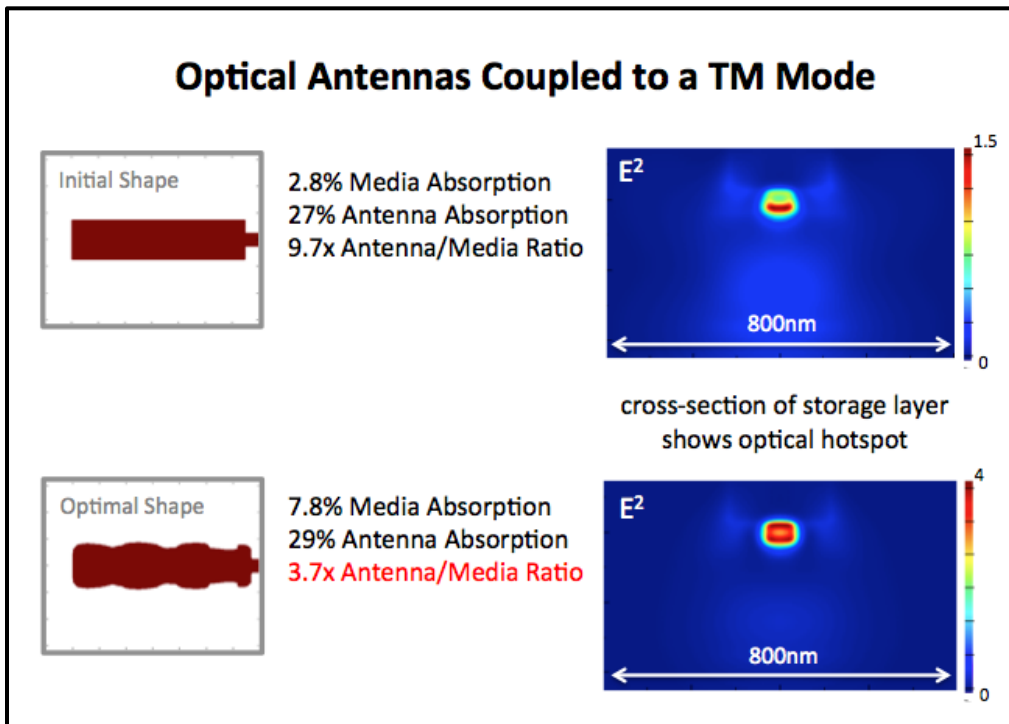


Figure 18: The initial and optimal shapes for an optical antenna coupled to a TM waveguide. On the right, electric field intensity through a cross-section of the storage medium is shown. Absorption more than doubles within the hotspot inside the storage layer, while the antenna's losses increase marginally.

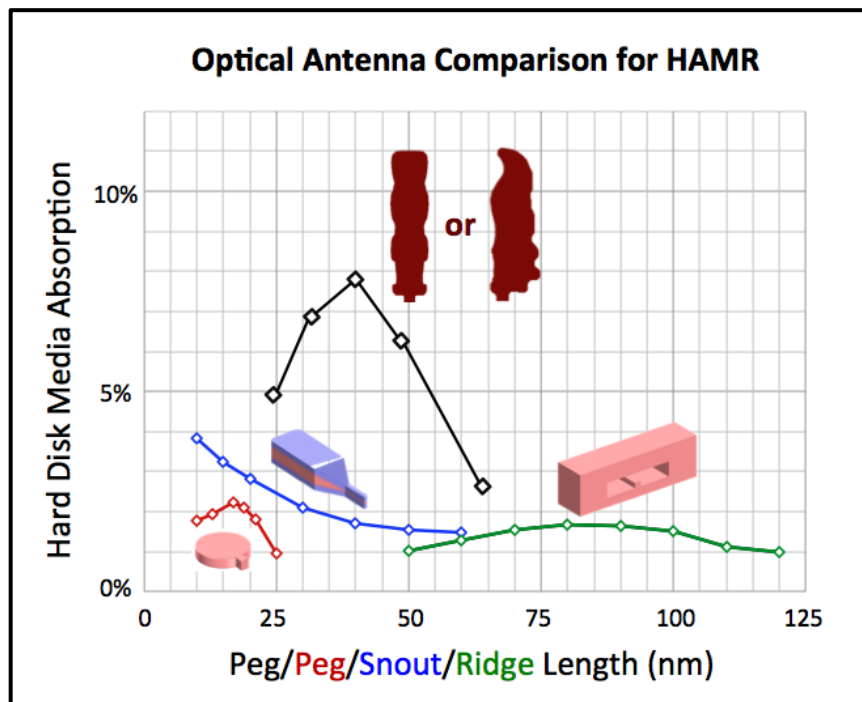


Figure 19: A comparison of the media coupling efficiency of the optical systems based on various optical antennas. For any HAMR antenna, the tip of the antenna is exposed to the air-bearing surface and is manufactured by lapping with a possible tolerance within +/- 10 nm.

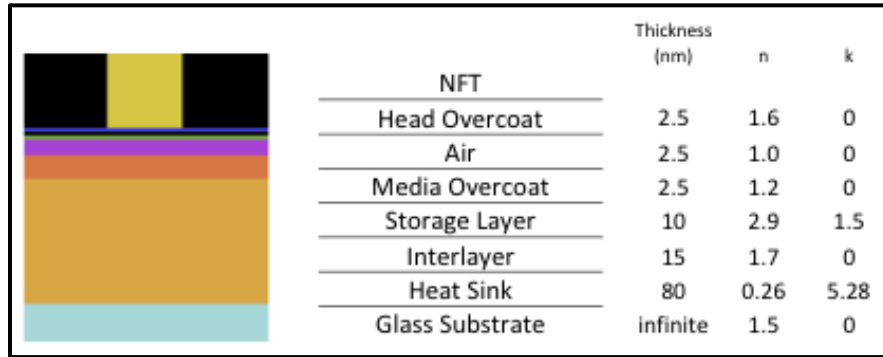


Figure 20: Important material properties for HAMR: Optical antenna or Near-Field Transducer (NFT), air bearing surface and various layers of the hard disk media.

4. Conclusion

The proposed Inverse Electromagnetic Design method of Adjoint-Based Gradient Descent is capable of very efficiently optimizing non-parametric shapes for many electromagnetic applications. The non-parametric approach is important to allow the optimization to exploit every degree of freedom possible and would require orders of magnitude more computation with traditional methods of optimization. It is thus capable of designing non-intuitive shapes that perform better than those designed by simple hand-analysis or parametric sweeps. Software developed to implement the Inverse Design method accompanied with a non-parametric geometry representation was successfully applied to the design of Optical Antennas for Heat-Assisted Magnetic Recording. This data-recording scheme requires the delivery of significant optical power to sub-wavelength spots with great efficiency, orders of magnitude greater than that of gold-coated optical fibers for Near-Field Optical Microscopes. The data storage industry has demonstrated very complicated approaches to HAMR, and instead a simple solution for HAMR was proposed here. The simple optical system merely consists of a rectangular waveguide and a planar optical antenna, which are easy to implement and manufacture. The Inverse Design software successfully designed the shapes of optical antennas (coupled to either TE or TM waveguide modes) that deliver ~8% of incident power to a small volume in the hard disk media, significantly outperforming previously-studied approaches.

5. References

- [1] Miller, “Photonic Design: From Fundamental Solar Cell Physics to Computational Inverse Design” UC Berkeley Dissertations (2012)
- [2] Jackson, “Classical Electrodynamics”, 3rd Edition, John Wiley and Sons Inc. (1999, 2004)
- [3] Wang, et. al., “Plasmonic Nearfield Scanning Probe with High Transmission” Nano Letters (2008)
- [4] Challener, “Light Delivery Techniques for Heat-Assisted Magnetic Recording” Jpn. Appl. Phys. (2003)
- [5] Challener, “HAMR by a near-field transducer with efficient optical energy transfer” Nature Photonics (2009)
- [6] Wu, “High-energy Electron Beam Lithography for Nanoscale Fabrication” InTech (2010)
- [7] Stipe, et. al., “Magnetic recoding at 1.5 Pb m^{-2} using an integrated plasmonic antenna” Nature Photonics (2010)
- [8] M Staffaroni, “Circuit Analysis in Metal-Optics, Theory and Applications” UC Berkeley Dissertations, (2011)
- [9] Johnson, “Perturbation theory for Maxwell’s equations with shifting material boundaries” Physical Review E (2002)
- [10] Johnson, “Roughness losses and volume-current methods in photonic-crystal waveguides” Applied Physics B (2005)
- [11] Fischetti, “Going Vertical: Perpendicular Recording” Scientific American (2006)